NURETH14-103

ANALYSIS OF THE NUPEC PSBT TESTS WITH FLICA-OVAP. PART 1: VOID DISTRIBUTION BENCHMARK

Philippe Fillion and Matteo Bucci

CEA DEN/Saclay DM2S/SFME
Laboratoire d'Etudes Thermohydrauliques des Réacteurs
91191 Gif sur Yvette Cedex, France
philippe.fillion@cea.fr, matteo.bucci@cea.fr

Abstract

Based on NUPEC PWR Subchannel and Bundle Tests (PSBT), an international benchmark has been promoted by OECD and NRC and has been coordinated by Penn State University (PSU). The benchmark includes void distribution and departure from nucleate boiling exercises. This paper is aimed at illustrating the capabilities of the full 3D thermal-hydraulic code FLICA-OVAP in predicting void distribution measurements available by the NUPEC tests. Subchannel and bundle test configurations have been analyzed. Both steady-state and transient scenarios have been addressed, including power increase, flow reduction, temperature increase and depressurization, representative of PWR thermal-hydraulics conditions. After a brief description of the main features of FLICA-OVAP, the relevant physical models available within the code are detailed. Results obtained in the different tests included in the PSBT void distribution benchmark are therefore reported. The relevant role of selected physical models is discussed.

1. Introduction

Based on NUPEC PWR Subchannel and Bundle Tests (PSBT), an international benchmark has been promoted by OECD and NRC and has been coordinated by Penn State University [1]. The aim of this benchmark is to encourage advancement and assessment of numerical models in subchannel analysis of fluid flow in rod bundles, which has very important relevance for the nuclear reactor safety margin evaluation. A important database of void fraction and critical heat flux measurements in steady-state and transient conditions have been carried out by NUPEC on a prototypical PWR rod bundle. Different types of subchannel or rod bundle geometries, and a wide range of flow conditions at high pressure have been investigated (see Table 1), allowing to assess the behavior of key models and correlations in these conditions.

The Laboratoire d'Etudes Thermohydrauliques des Réacteurs (LETR) at the Commissariat à l'Energie Atomique et aux Energies Alternatives (CEA), France, is involved in the PSBT benchmark performing calculations with the FLICA-OVAP code. FLICA-OVAP is an advanced two-phase flow thermal-hydraulics code based on a full 3D subchannel approach [2]. It is designed to analyze flows in Light Water Reactors cores such as PWRs, BWRs and experimental reactors.

Table 1: Operation conditions of the NUPEC PWR test facility

| Quantity | Range |
|---------------------------|---------------------------------------|
| Pressure | 4.9 - 16.6 MPa |
| Mass velocity | $550 - 4150 \text{ kg/(m}^2\text{s})$ |
| Inlet coolant temperature | 140 - 345°C |
| Wall heat flux | $0.37 - 1.86 \text{MW/m}^2$ |

To provide a relevant answer to different core concepts and multiple industrial applications, several models coexist in the FLICA-OVAP platform: the Homogeneous Equilibrium model, the drift flux model, the two-fluid model, and finally, a general multifield model, with a variable number of fields for both vapor and liquid phases. For each model, an adapted set of closure laws is proposed concerning mass and heat transfer, interfacial and wall forces, and turbulence. The four-equation drift-flux model and the most correlations (wall transfer, mass exchange, ...) used for this benchmark comes directly from FLICA-4 code [3] and has been validated for PWR studies [4]. Correlations and parameters will be assessed on the test matrix proposed by the benchmark.

2. Description of the FLICA-OVAP code

2.1. Physical modelling

For the sake of simplicity the four-equation drift-flux model is presented here without taking into account porosity. The three balance equations for the mixture read:

• mixture mass conservation

$$\frac{\partial}{\partial t} \left(\sum_{k=\nu,\ell} \alpha_k \rho_k \right) + \nabla \cdot \left(\sum_{k=\nu,\ell} \alpha_k \rho_k \mathbf{u}_k \right) = 0, \tag{1}$$

mixture momentum balance

$$\frac{\partial}{\partial t} \left(\sum_{k=v,\ell} \alpha_k \rho_k \mathbf{u}_k \right) + \nabla \cdot \left(\sum_{k=v,\ell} \alpha_k \rho_k \mathbf{u}_k \otimes \mathbf{u}_k \right) + \nabla P - \nabla \cdot \left(\sum_{k=v,\ell} \alpha_k \underline{\underline{\tau}_k} \right) = \rho \mathbf{g} + \mathbf{F}_w$$
 (2)

mixture energy balance

$$\frac{\partial}{\partial t} \left(\sum_{k=\nu,\ell} \alpha_k \rho_k E_k \right) + \nabla \cdot \left(\sum_{k=\nu,\ell} \alpha_k \rho_k H_k \mathbf{u}_k \right) - \nabla \cdot \left(\sum_{k=\nu,\ell} \alpha_k \mathbf{q}_k \right) = q_w + \rho \mathbf{g} \cdot \mathbf{u}$$
(3)

Thermal disequilibrium is taken into account by an additional balance equation:

$$\frac{\partial}{\partial t}(\alpha_{\nu}\rho_{\nu}) + \nabla \cdot (\alpha_{\nu}\rho_{\nu}\mathbf{u}_{\nu}) - \nabla \cdot (K_{c}\nabla c) = \Gamma_{\nu}$$
(4)

In these equations, α_k , ρ_k , \mathbf{u}_k , E_k , H_k are respectively volume fraction, density, velocity, total energy and total enthalpy for the phase k. P is the pressure, $\rho = \sum_{k=\nu,\ell} \alpha_k \rho_k$ the mixture density,

 $c = \alpha_v \rho_v / \rho$ is the vapor concentration, **g** the gravity vector, \mathbf{F}_w the friction forces and $\mathbf{u} = \sum_{k=v,\ell} \alpha_k \rho_k \mathbf{u}_k$ is the mixture velocity. K_c represents a diffusion term for the concentration and $\underline{\tau}_k$ the viscous and Reynolds stress terms for the phase k. \mathbf{q}_k includes molecular and turbulent heat fluxes, and q_w is the volumetric source term of thermal power. Γ_v is the mass transfer term, which will be better defined later. The model is closed by a general equation of state for each phase:

$$\rho_k = \rho_k(P, h_k), \quad \text{for} \quad k = \nu, \ell$$
(5)

and by the assumption that the vapor is saturated in presence of liquid. The vapor specific enthalpy h_v is thus given by the saturated steam enthalpy at the system pressure P

$$h_{v} = h_{v,\text{sat}}(P) \tag{6}$$

Drift-flux correlations. FLICA-OVAP includes several Zuber-Findlay type correlations in order to estimate the relative velocity $\mathbf{u}_r = \mathbf{u}_v - \mathbf{u}_\ell$ between vapor and liquid phases. Chexal-Lellouche correlation [5] and a correlation derived from Ishii [6] are implemented because they are suitable for many flows conditions: the Chexal and Lellouche correlation covers a full range of pressure, diameters, flows and the Ishii correlation, first establish for bubbly, slug and churn-turbulent flow in adiabatic conditions, takes also into account the nucleate boiling on heated walls in the formulation used for this benchmark.

Wall heat transfer Nusselt number and bulk temperature are defined according to the heat transfer regime. In particular, three different regimes can be distinguished for the void distribution benchmark: single-phase convection heat transfer, subcooled nucleate boiling (SNB) and saturated nucleate boiling (SANB).

In single-phase heat transfer and subcooled nucleate boiling, the bulk temperature is equal to the liquid phase temperature, whereas in saturated nucleate boiling it coincides with the saturation temperature. The single-phase heat transfer coefficient is obtained by the Dittus-Boelter correlation. The onset of significant void (OSV), that is the transition between single-phase heat transfer and subcooled nucleate boiling (SNB) is predicted according to Jens and Lottes correlation [7], which allows estimating the minimum wall superheating $\Delta T_{\rm sat}$ demanded to achieve net vapor generation:

$$\Delta T_{\text{sat}} = 7.91 \left(\frac{q''}{10^4}\right)^{0.25} \exp\left(\frac{-P}{62.10^5}\right),$$
 (7)

where q'' is the wall heat flux and all the quantities are expressed in SI units. This correlation is valid in the following range: 0.7 < P < 17.2 MPa, 115 < water temperature < 340°C, q'' < 12.5 MW m⁻², 11 < G < 10500 kg/(m²s). When the wall temperature estimated by the Dittus-Boelter correlation exceeds this value, vapor generation onsets at walls and the wall temperature is estimated by the Jens and Lottes model.

Mass transfers. In equation (4), the mass exchange Γ_{ν} is the sum of the vapor generation on the wall $\Gamma_{\nu\nu}$ and the evaporation or condensation within the bulk flow $\Gamma_{\nu\ell}$.

The vapor generation at walls is given by:

$$\Gamma_{wv} = \frac{\chi q''}{h_{v,\text{sat}} - h_{\ell,\text{sat}}} \frac{4}{D_{\text{heat}}}$$
(8)

where D_{heat} is the heated diameter and χ is the fraction of the wall heat flux used to vaporize the liquid and consequently $1-\chi$ is the fraction used to heat the subcooled liquid. $h_{\nu,\text{sat}}$ and $h_{\ell,\text{sat}}$ are respectively the saturated steam enthalpy and the saturated liquid enthalpy at the system pressure. If the liquid is in saturation conditions, χ is set equal to 1. In subcooled boiling, χ is given by:

$$\chi = \frac{T_{w,lc} - T_{\text{sat}} - \Delta T_{\text{sat}}}{T_{w,lc} - T_l - \Delta T_{\text{sat}}}$$
(9)

in the subcooled boiling region, where $T_{w,lc}$ is the wall temperature given by the liquid convective heat transfer.

The evaporation or condensation within the bulk flow is given by

$$\Gamma_{\nu\ell} = \frac{q_{\nu\ell}}{h_{\nu} - h_{\ell}} \tag{10}$$

where $q_{v\ell}$ is the heat transfer rate between the phases, h_v is the vapor enthalpy (equal to $h_{v,sat}$) and h_{ℓ} is the actual liquid enthalpy. In the two-phase region, $q_{v\ell}$ formulation is:

$$q_{\nu\ell} = K_{\nu 0} \frac{G^2}{\log(1 + \text{Re}/\text{Re}_0)} f(P, \rho, \mu_\ell, \mathbf{u}, \mathbf{u}_r) \frac{\rho c(x_{\text{eq}} - c)}{1 - c}$$

$$\tag{11}$$

where $K_{\nu 0}$ is a constant, G the mass flux, $\text{Re} = GD_h/\mu_\ell$ is the Reynolds number, x_{eq} the equilibrium quality, $f(P, \rho, \mu_\ell, \mathbf{u}, \mathbf{u}_r)$ a function depending on local conditions, D_h is the hydraulic diameter and μ_ℓ the liquid viscosity. Re₀ is a parameter of the model.

Pressure drops. The friction \mathbf{F}_w is the sum of the singular friction due to the assembly grids or other pressure drops \mathbf{F}_{sing}

$$\mathbf{F}_{\text{sing}} = -\frac{1}{2}\rho \underline{\mathbf{K}}_{\text{sing}} ||\mathbf{u}||\mathbf{u}$$
 (12)

where $\underline{\underline{\mathbf{K}}}_{sing}$ is an antisymmetric tensor, and the distributed friction on wall \mathbf{F}_{frict} :

$$\mathbf{F}_{\text{frict}} = -\frac{1}{2D_h} \rho f_w ||\mathbf{u}|| \mathbf{u}$$
(13)

The friction term in equation (13) is divided into three components: an isothermal friction factor f_{iso} , a heating wall correction factor f_{heat} and the two-phase multiplier $f_{2\phi}$.

$$f_w = f_{\rm iso} \times f_{\rm heat} \times f_{2\phi} \tag{14}$$

The isothermal friction factor depends on the flow regime; in turbulent flows it is modeled as

$$f_{\rm iso} = 0.194 \text{Re}^{-0.2} \tag{15}$$

The two-phase flow multiplier in FLICA-OVAP is of the form:

$$f_{2\phi} = 1 + (\phi_{\ell o}^2 - 1) \left(1 + \frac{D_{\text{heat}}}{D_h} C_{\phi} q'' \right)$$
 (16)

where $\phi_{\ell o}^2$ is the adiabatic two-phase frictional pressure drop multiplier, C_{ϕ} a constant accounting for heat flux and D_{heat} is the heated diameter. In the runs of the PSBT benchmark C_{ϕ} was taken equal to 0 and thus $f_{2\phi} = \phi_{\ell o}^2$.

Diffusion effects. The tensor $\underline{\tau_k}$ for viscous and turbulent effects is defined for each phase by:

$$\tau_k^{ij} = \mu_k (1 + M_{t,k}^{ij}) \left(\frac{\partial u_k^i}{\partial x_j} + \frac{\partial u_k^j}{\partial x_i} - \frac{2}{3} \sum_{l=x,y,z} \frac{\partial u_k^l}{x_l} \delta_{ij} \right)$$
(17)

where $\mu_k M_{t,k}^{ij}$ is a turbulent viscosity (*i* and *j* account mutually for the *x*, *y*, and *z* directions). In practice, the turbulent viscosity is only taken into account for the liquid phase. The anisotropic formulation used for turbulent conditions is:

$$M_{t,\ell}^{ij} = M_{t0}^{ij} \left(\text{Re} - \text{Re}_t \right)^{b_M} f_M(f_{2\phi})$$
 (18)

where M_{t0}^{ij} , Re_t and b_M are coefficients and $f_M(f_{2\phi})$ a function depending on the two-phase frictional multiplier.

The molecular and turbulent heat fluxes are written as:

$$\sum_{k=\nu,\ell} \alpha_k \mathbf{q}_k = \frac{\lambda_\ell}{C_{p_\ell}} (\underline{\underline{\mathbf{1}}} + \underline{\underline{\mathbf{K}}}_{t,\ell}) \nabla h_x \tag{19}$$

where $h_x = xh_v + (1-x)h_\ell$ is the flow enthalpy based on the quality x. The formulation of the turbulent conductivity coefficients $K_{t\ell}^{ij}$ is:

$$K_{t,\ell}^{ij} = K_{t0}^{ij} (\text{Re} - \text{Re}_t)^{b_K} f_K(f_{2\phi})$$
 (20)

where K_{t0}^{ij} and b_K are coefficients. In equations (20) and (18), b_M , b_K , f_M and f_K are set to 1. In the following simulations, K_{t0} and K_c (see eq. (4)) coefficients are equal. This means that the turbulent diffusion velocity scale for the energy is approximated equal to the diffusion velocity scale for the steam species.

2.2. Numerical methods

The equations are solved with colocated finite volume type schemes. These schemes allow to solve the system on any type of structured or unstructured mesh that can be either conforming or non-conforming. The hyperbolic part of the system is approximated with a VFRoe-type scheme modified to be accurate at low Mach number. The diffusion part of the system is approximated with a *diamond* technique. Further details of the numerical methods can be found in [2].

3. Void distribution results

3.1. Subchannel exercises

Four series of measurements of the void fraction were performed in sections representative of the subchannel types found in a PWR assembly. Table 2 gives the geometry (center typical and thimble subchannels, side and corner subchannels) and power shape for these series. The heated length is 1555 mm, and the void measurement section is located at 1400 mm from the bottom of the heated section.

| Item | Data | | | |
|--------------------------|------------------|------------------|---------|---------|
| Assembly | S1 | S2 | S3 | S4 |
| (subjected subchannel) | | | | |
| Subchannel type | Center (Typical) | Center (Thimble) | Side | Corner |
| Number of heaters | 4 x 1/4 | 3 x 1/4 | 2 x 1/4 | 1 x 1/4 |
| Axial heated length (mm) | 1555 | 1555 | 1555 | 1555 |
| Axial power shape | Uniform | Uniform | Uniform | Uniform |
| Number of runs | 43 | 43 | 20 | 20 |

Table 2: Geometry and power shape of rod bundle test assembly (from [8])

With the given test matrix (power value and boundary conditions), the flow is saturated at the measurement location of the void fraction for the most runs. So, this situation allow only partial assessment of the subcooled boiling models. In contrast, drift flux model plays a major role to obtain good agreement with experimental data. Chexal-Lellouche and Ishii correlations have been compared for series 1 (Fig. 1): Ishii correlation tends to under-predict the void fraction more than Chexal-Lellouche. For this reason, even if it is not obvious to extend this conclusion to other configurations, the Chexal-Lellouche correlation has been preferred for other subchannel and bundle calculations.

Calculated densities and void fractions are compared against the experimental data (Fig. 2). Experimental densities measured by CT scan are declared to be affected by an uncertainty of 15 kg/m³ ($\sigma_{exp} = 15 \text{ kg/m}^3$) [8]. Experimental void fraction resumed basing on measured densities are presumed to be affected by an uncertainty of 3% of void fraction ($\sigma_{exp} = 3\%$ in Figure 2) [8]. It happens that densities obtained by the code match well the experimental ones, whereas void fractions are slightly under-estimated for the lowest value of this quantity. Indeed, physical properties and correlations adopted to convert density to void fraction could be the cause for this discrepancy.

3.2. Rod bundle exercises

A partial section of the full length 17x17 type PWR fuel assemblies was considered. The rod bundle test is a 5x5 square array. The heated section is 3658 mm high, and density measurements are set at 2216 mm (Lower), 2669 mm (Middle), and 3177 mm (Upper). The gamma-ray

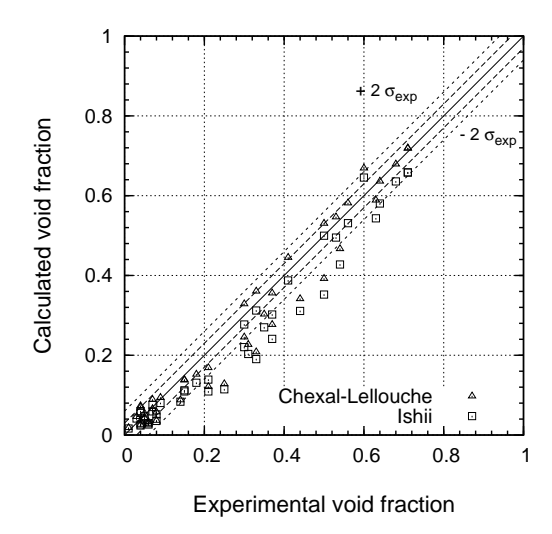


Figure 1: Subchannel S1 series. Comparison of the Chexal-Lellouche and Ishii drift correlations prediction with experimental data.

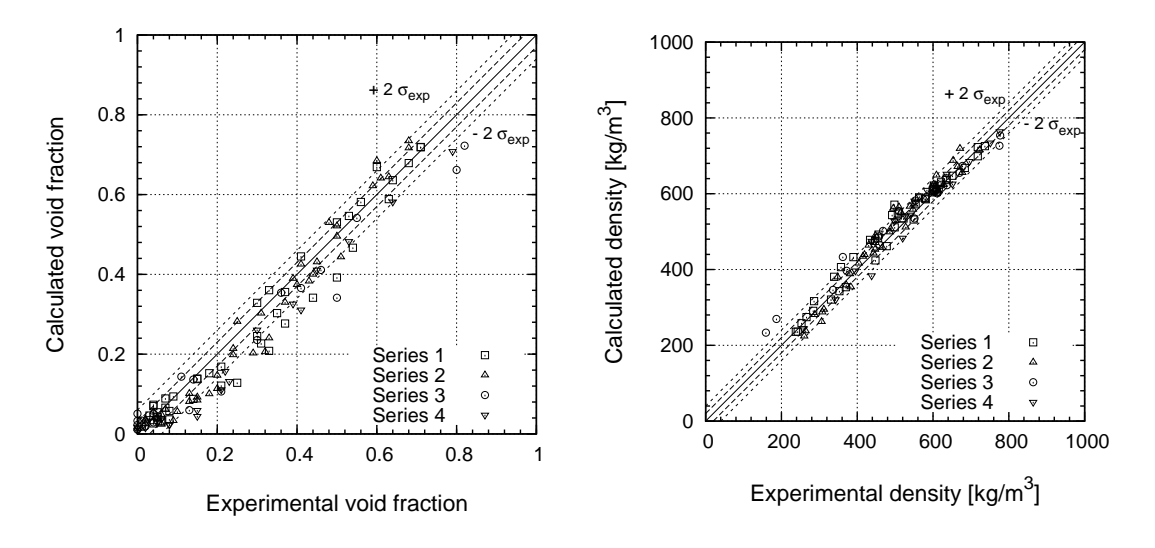


Figure 2: Subchannel exercises. Calculated void fraction and density vs. experimental data for series 1 to 4 with Chexal-Lellouche drift correlation.

transmission method (Chordal Averaged) was adopted in the tests performed to measure the density, and then converted to the void fraction of the gas-liquid two-phase flow. The declared uncertainties are 4% of void fraction ($\sigma_{exp}=4\%$ in Figure 3 and Figure 4) for steady-state bundle tests and 5% of void fraction ($\sigma_{exp}=5\%$ in Figure 5 and Figure 6) for transient bundle tests. In Table 3 are shown the geometry and power shape of the rod bundle test assemblies considered.

Three assembly configurations were considered: B5, B6, and B7 (see Table 3). The main difference between these three configurations is in the power distribution. Assembly B5 has a uniform axial power distribution and pattern A radial power distribution. Assembly B6 has the same radial power distribution of assembly B5 but cosine axial power distribution. Assembly B7 has a cosine axial power distribution and pattern B radial power distribution. For this radial power distribution, the central rod is a thimble rod (i.e., no power is generated inside this rod) of larger diameter with respect to the fuel rods as shown in Table 3.

Table 3: Geometry and power shape of rod bundle test assembly (from [1])

| Item | Data | | | |
|-------------------------------------|---|--|--|--|
| Assembly | B5 | B6 | B7 | |
| Rods array | 5 x 5 | 5 x 5 | 5 x 5 | |
| Number of heated rods | 25 | 25 | 24 | |
| Number of thimble rods | 0 | 0 | 1 | |
| Heated rod outer diameter (mm) | 9.50 | 9.50 | 9.50 | |
| Thimble rod outer diameter (mm) | - | - | 12.24 | |
| Heated rods pitch (mm) | 12.60 | 12.60 | 12.60 | |
| Axial heated length (mm) | 3658 | 3658 | 3658 | |
| Flow channel inner width (mm) | 64.9 64.9 | | 64.9 | |
| Radial power shape | pattern A | | pattern B | |
| | 0.85 1.00 1.0 0.85 1.00 1.0 0.85 0.85 0.85 0.85 | 00 1.00 0.85 00 1.00 0.85 00 1.00 0.85 85 0.85 0.85 | 0.85 0.85 0.85 0.85 0.85 0.85 1.00 1.00 1.00 0.85 0.85 1.00 0.00 1.00 0.85 0.85 1.00 1.00 1.00 0.85 0.85 0.85 0.85 0.85 0.85 | |
| Axial power shape | Uniform | Cosine | Cosine | |
| Number of mixing vane spacers | 7 | 7 | 7 | |
| Number of no mixing vane spacers | 2 | 2 | 2 | |
| Number of simple spacers | 8 8 | | 8 | |
| Mixing vane spacer location (mm) | 471, 925, 1378, 1832, 2285, 2739, 3247 | | | |
| (Loss coefficient 1.0 [1]) | from the beginning of the heated section | | | |
| No mixing vane spacer location (mm) | 2.5, 3755 | | | |
| (Loss coefficient 0.7 [1]) | from the beginning of the heated section | | | |
| Simple spacer location (mm) | 237, 698, 1151, 1605, 2059, 2512, 2993, 3501 | | | |
| (Loss coefficient 0.4 [1]) | from the beginning of the heated section | | | |

In Table 4 are shown the test series for void fraction measurements.

| Test series | Assembly | Test mode | |
|-------------|----------|--------------|-----------|
| | | Steady-state | Transient |
| 5 | B5 | 74 runs | |
| 5T | | | 4 runs |
| 6 | В6 | 74 runs | |
| 6T | | | 4 runs |
| 7 | В7 | 74 runs | |
| 7T | | | 4 runs |
| 8 | В5 | 31 runs | - |

Table 4: Test series for void fraction measurements

3.2.1. Steady state exercises

For the results at the lower and middle elevations, subcooled nucleate boiling models (condensation and wall heat transfer) play a major role for the prediction of the void fraction. At the upper elevation, the fluid is generally saturated, and the drift model becomes important. Moreover, diffusion terms play also a major role, and turbulent diffusion promoted by the presence of mixing grid spacers must be taken into account. Standard parameters $K_{t0}^{ij}(z) = k_{tb}$ and $M_{t0}^{ij}(z) = m_{tb}$ (the turbulent Prandtl number is assumed equal to 1) adopted for bare bundles (without any spacer) have to be increased in the region upstream mixing grid spacers in order to reproduce the enhancement of turbulent mixing. In equations (20) and (18), K_{t0}^{ij} and M_{t0}^{ij} have been therefore adapted for the PSBT assemblies by means of piecewise functions: it was assumed that $K_{t0}^{ij}(z) = k_{ts}$ and $M_{t0}^{ij}(z) = m_{ts}$ downstream a mixing grid spacer, instead of taking the standard values k_{tb} and m_{tb} . Despite the value of k_{tb} and m_{tb} is reliably assessed to be around 0.010 for PWR type bundles, the appropriate values to be adopted for k_{ts} and m_{ts} are not known for these particular mixing grid spacers and thus a sensitivity analysis has been performed to better identify reasonable values for these coefficients.

Sensitivity analysis of coefficients K_{v0} of the condensation model and of coefficients m_{tb} and m_{ts} (or k_{tb} and k_{ts}) were also conducted. A sample result is shown in Figure 3, where the effect of these parameters are reported for run 5.2442. In the subcooled and at the beginning of the saturated region, void fraction is strongly reduced as K_{v0} value increases, but this parameter does not effect results at the end of the bundle, where the flow is fully saturated. On the other hand, effect of the turbulent diffusion coefficients k_{ts} and m_{ts} is significant when the void fraction increases, since it determines the flatness of the void distribution profile in the bundle. Detailed experimental density maps would have been useful to assess a reliable value for the turbulent diffusion coefficients, but these maps are not readily exploitable. As far as we could deduce basing on the void fraction profile in the central subchannel, a value for k_{ts} and m_{ts} was chosen equal to 0.045. The value of K_{v0} was instead taken equal to 1.5 × 10⁴, which is in the standard range of values adopted in thermal-hydraulic analysis performed with this model.

Figures 4 (a), (b) and (c) show the calculated void fraction against the experimental values for series 5, 6 and 7, with the following parameters: $K_{v0} = 1.5 \times 10^4$, $k_{ts} = m_{ts} = 0.045$, $k_{tb} = m_{tb} = 0.01$.

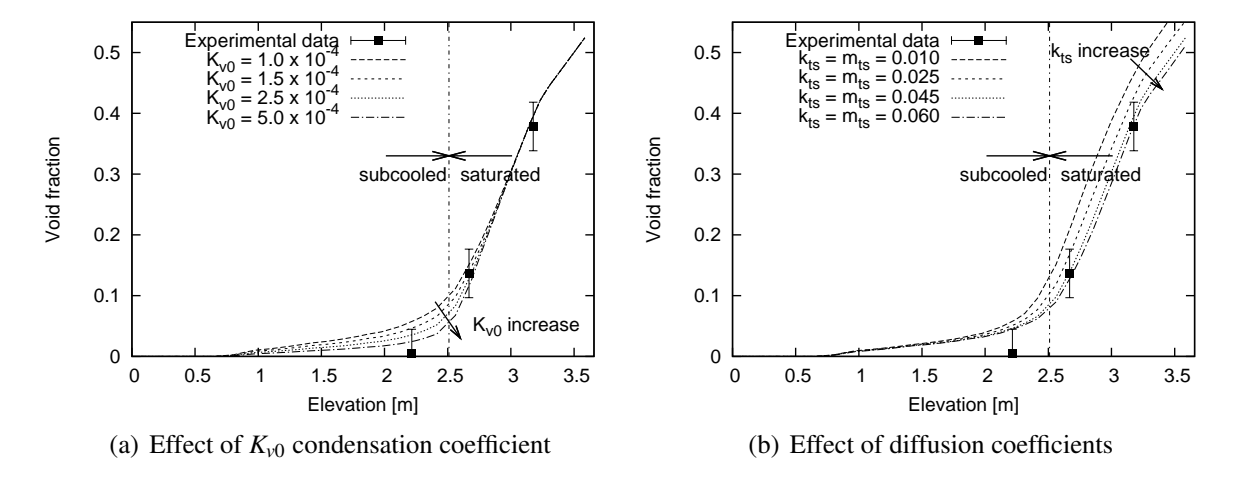


Figure 3: PSBT run 5.2442. Sensitivity analysis of coefficients K_{v0} , k_{ts} and m_{ts} : effect on the void fraction profile of the central subchannel.

For all series, at the lower and middle elevations, the code tends to slightly over-predict the void fraction, whereas at the upper elevation the discrepancy between calculated and measured void fraction is generally included within the range of uncertainty declared for the measurements $\pm 2\sigma_{exp}$, with $\sigma_{exp} = 4\%$.

3.2.2. Transient exercises

For the transient simulations, three different configurations were taken into account as shown in Table 4. Test series 5T considers the same assembly conditions used for steady-state test series 5, which are uniform axial power distribution, and pattern A radial power distribution. For transient test series 6T the same assembly conditions used for steady-state test series 6 were applied, which means a cosine axial power distribution, and pattern A radial power distribution. Test series 7T considers the same assembly conditions used for steady-state test series 7, which are cosine axial power distribution, and pattern B radial power distribution.

For each transient analysis, four different scenarios were considered: power increase, flow reduction, depressurization, and temperature increase. Boundary conditions were provided for each scenario, using table where the dependent variables (i.e., power, pressure, mass flux, and inlet temperature respectively) were specified as function of the simulation time. Same parameters and model as for steady-state bundle computations were used.

Figure 5 shows complete results for transients 5T, also representative of the other transient series 6T and 7T. FLICA-OVAP presents a good agreement against the experimental void fraction for all transients, except for the temperature increase transient. For the power increase transient, the evolution of the void fraction follows the data, but the void fraction is under-estimated at the middle and upper locations. The results concerning the depressurization have more discrepancy as time increases, but are consistent with the experimental evolution.

For the temperature increase transient, a shift of calculated void fractions profiles with respect to experimental values can be noticed. This discrepancy have been noticed by several participants

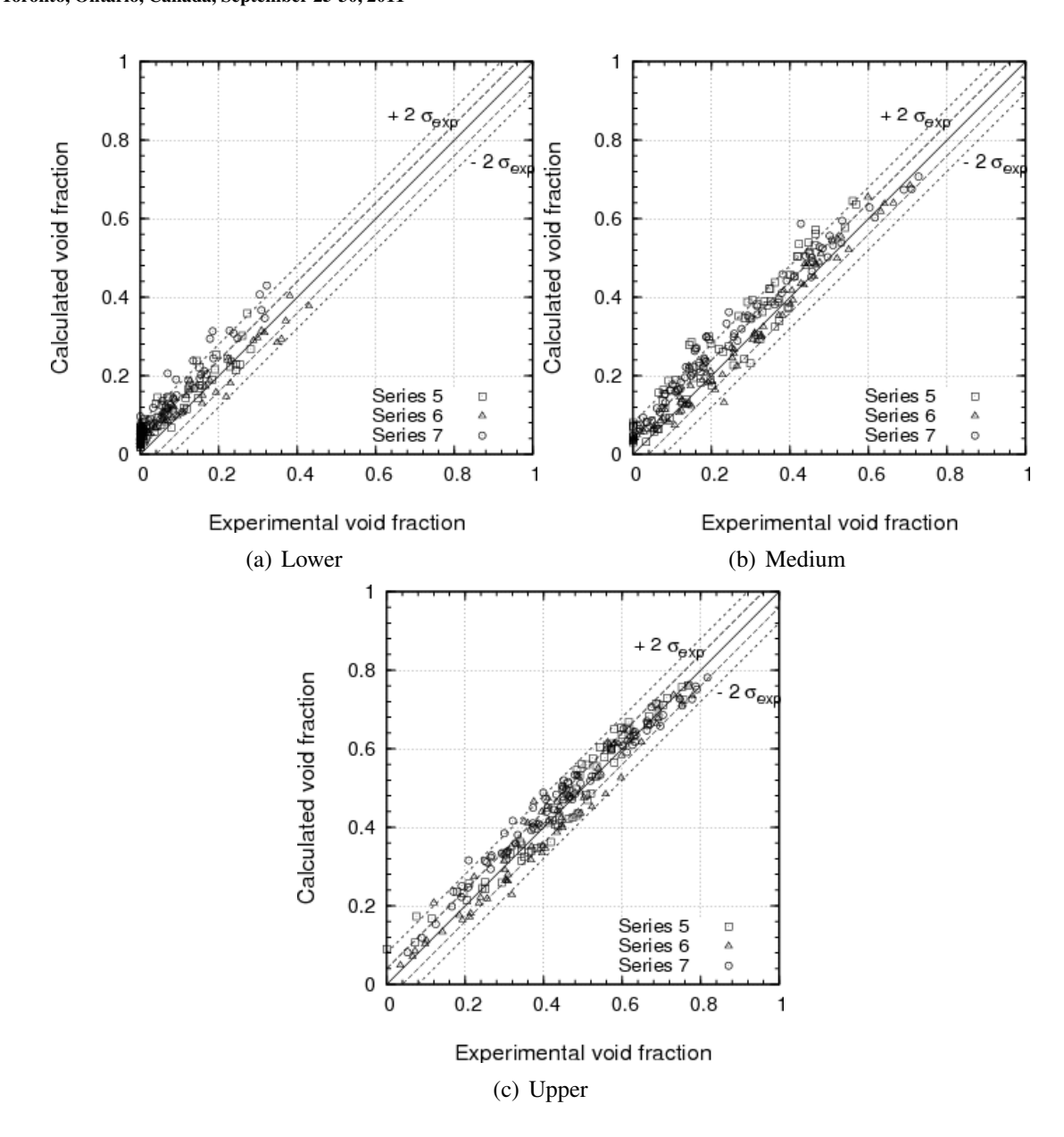


Figure 4: Steady state rod bundle exercises. Comparison of calculated void fraction profiles in the central subchannel against the experimental data.

to the first PSBT/OECD workshop in Pisa. Fluid temperature probe is located in a pipe between the pre-heater and the inlet nozzle of the test section [8]. It is therefore reasonable to affirm that a delay of several seconds occurs between the measurement point and the inlet of the heated section. This point has been investigated by JNES [8] but the distance from the measurement location to the inlet of the heated section (where the temperature boundary condition has to be applied in thermal-hydraulics codes) was not clarified. As far as we can say basing on the result obtained by FLICA-OVAP, if a delay of 6 s is taken for the inlet temperature with respect to other boundary conditions (i.e. the initial temperature is maintained during 6 s and

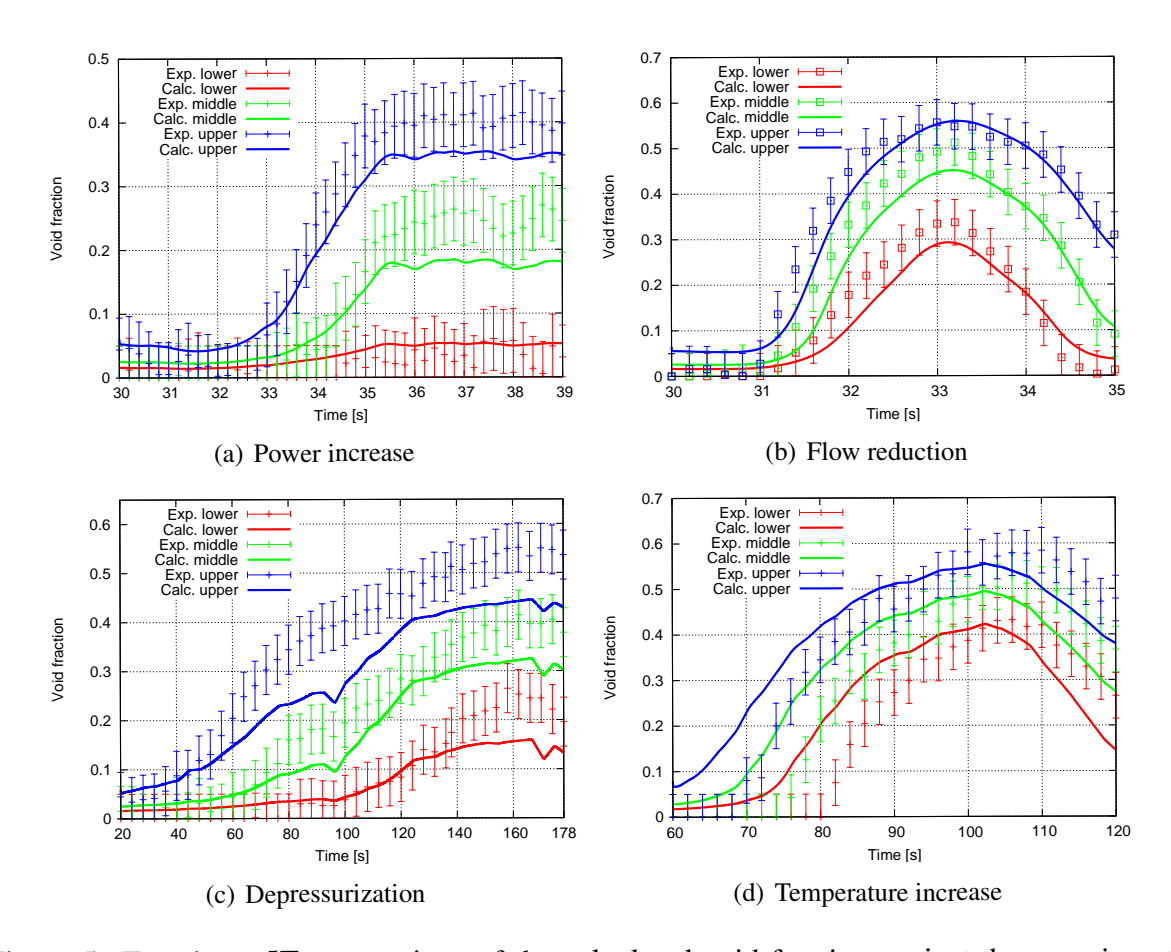


Figure 5: Transients 5T: comparison of the calculated void fraction against the experimental void fraction.

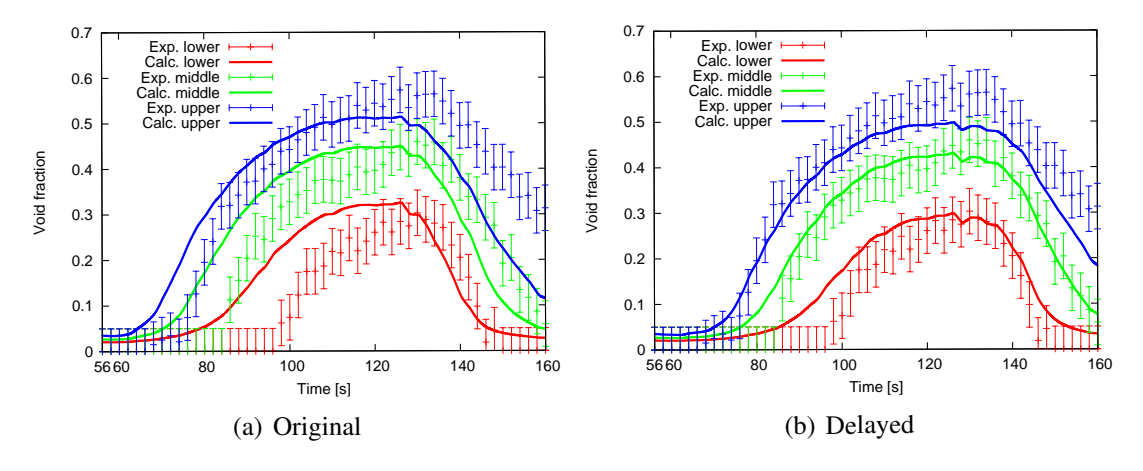


Figure 6: Original and Delayed temperature boundary conditions in the temperature increase 6T transients

then the temperature variation is applied), the agreement between calculated and experimental void fraction profiles is improved. It can clearly be seen in Figure 6, where these profiles are

compared for the calculations with and without the time delay of 6 seconds.

4. Conclusions

An analysis of the void distribution tests addressed in the frame of the OECD/NRC PSBT benchmark has been proposed. The drift-flux model of the FLICA-OVAP code and its main physical models have been assessed against void distribution data released by NUPEC. Experimental data consist of steady-state void fraction measurements in different subchannel configurations and steady-state and transient axial void fraction distribution in bundle configuration (three axial measurement points in the central subchannel of the bundle).

Void fraction measurements in the subchannel configurations are of major interest for the validation of mass transfer model and the OSV criterion. In this analysis, the attention was focused on the mass transfer model, but further improvement of this work could include the analysis of other OSV criteria. Results obtained by FLICA-OVAP with a set of standard coefficients for the different models show a good agreement of the calculated densities and a slight underestimation of the void fraction at the measurement location, mainly located in the saturated regime for the considered runs.

For the steady-state bundle tests, the K_{v0} coefficient and diffusion coefficients k_t and m_t are the key parameters to fit the void fraction. In particular, mixing grid spacers play a major role, since they are due to enhance the turbulence in the downstream flow. It was found that a reasonably good agreement between calculated and experimental void fraction profiles is achieved when the turbulent diffusion associated to mixing grid is taken equal to $k_{ts} = m_{ts} = 0.045$.

Adopting the same set of parameters, a reasonably good agreement between calculated and experimental void fraction was also ascertained for transient tests, even if a systematic underestimation of void fraction at the middle and upper measurement locations has been found. Discrepancies noticed on temperature increase transients were corrected by applying a delay of 6 s of the original inlet temperature boundary conditions, in order to simulate the residence time of the fluid between the temperature probe where the boundary conditions is given and the inlet of the test section.

Results obtained on the subcooled region suggest possible directions to be pursued in order to improve the current modeling: further developments and validation will involve the OSV criterion and the modeling of heat flux and heat flux partitioning in subcooled nucleate boiling, but also the modeling of inter-phase mass transfer and turbulent diffusion terms.

Acknowledgments

The authors would like to thanks Angelo Frisani (Texas A&M University) and Anela Kumbaro (CEA) for their contributions in the analysis of the NUPEC PSBT tests.

References

[1] A. Rubin, A. Schoedel, M. Avramava, H. Utsuno, S. Bajorek, and A. Velazquez-Lozada, "OECD/NRC benchmark based on NUPEC PWR subchannel and bundle tests

- (PSBT). Volume I: Experimental Database and Final Problem Specifications," Tech. Rep. NEA/NSC/DOC(2010)1, NEA/NSC, Nov. (2010).
- [2] P. Fillion, A. Chanoine, S. Dellacherie, and A. Kumbaro, "FLICA-OVAP: a New Platform for Core Thermal-hydraulic Studies," in *Proceedings of NURETH-13*, Kanazawa, Japan, Sep. 26 Oct. 2 (2009).
- [3] E. Royer, S. Aniel, A. Bergeron, P. Fillion, D. Gallo, F. Gaudier, O. Grégoire, M. Martin, E. Richebois, P. Salvadore, S. Zimmer, T. Chataing, P. Clément, and F. François, "FLICA4: Status of numerical and physical models and overview of applications," in *Proceedings of NURETH-11*, Avignon, France, October 2-6 (2005).
- [4] M. Bucci, A. Charmeau, and P. Fillion, "FLICA-OVAP: Elements of validation for LWRs thermal-hydraulic studies," in *Proceedings of ICAPP 2011*, Nice, France, May 2-5 (2011).
- [5] B. Chexal, G. Lellouche, J. Horowitz, and J. Healzer, "A Void Fraction Correlation for Generalized Applications," *Progress In Nuclear Research*, **27**, no. 4, pp. 255–295, (1992).
- [6] M. Ishii, "One dimensional drift-flux model and constitutive equations for relative motion between phases in various two-phase flow," Tech. Rep. ANL-77-27, ANL, (1977).
- [7] W. Jens and P. Lottes, "Analysis of heat transfer burnout, pressure drop and density data for high pressure water," Tech. Rep. ANL-4627, ANL, (1951).
- [8] H. Utsuno, "OECD/NRC benchmark based on NUPEC PWR subchannel and bundle tests (PSBT). Assembly Specification and Benchmark Database. Volume I Addendum," Tech. Rep. JNES/SAE-TH08-0019 (Addendum), JNES, (2010).